Peer-reviewed version available at *Electronics* **2020**, *9*, 1350; doi:10.3390/electronics9091350

Multiband Dual-Meander Line Antenna for Body Centric Networks Biomedical Applications by Using UMC 180 nm

Hala Shawkey and Dalia Elshaekh
heba_shawkey@eri.sci.eg and daliaelsheakh@eri.sci.eg
Electronics Research Institute, El Dokki, Giza, Egypt, 12622.
Corresponding author-email daliaelsheakh@eri.sci.eg

Abstract

This paper presents a compact on-chip antenna architecture for 5G body centric networks (BCNs) applications. A dual meander line (DML) integrated antenna consists of two stacked layers of two turns of meander lines and a ground metal layer. The DML structure decreases the resonant frequency, increases tuning bands and broadens the operating bandwidth to be a suitable choice for high data rate biomedical applications. The antenna's performance is evaluated in both scenarios inside and outside the human body. The proposed antenna is fabricated using UMC180 nm CMOS technology with a total area of 1150µm×200µm, and operates at bands 22 GHz, 34 GHz, 44 GHz and 58 GHz with an operating bandwidth up to 2 GHz at impedance bandwidth ≤ 7.5 dB (VSWR≤2.5). The proposed antenna is simulated using high frequency structure simulator (HFSS) and shows good agreement between measured and simulated results.

Keywords: integrated antenna; meander line (ML); 5G technology; body centric networks (BCNs); WBAN; WSN; WPAN; UMC 180nm CMOS

1. Introduction

5G technologies have the potential to make significant contributions to providing secure healthcare-orientated wireless networks with improved energy efficiency. Ultra-wideband (UWB) communication becomes the solution of the higher demand capacity to

Peer-reviewed version available at Electronics 2020, 9, 1350; doi:10.3390/electronics9091350

multiple devices in 5G technology. UWB is a key component in many applications as radar imaging and smart biomedical sensors, which can be worn or implanted in the human-body [1-3]. Recently, these biosensors created closed UWB wireless body centric networks (BCNs) as shown in Fig.1 [4]. Body-centric wireless communications refer to human-self and human-to-human networking with the use of wearable and implantable wireless sensors. BCNs is a subject area combining wireless body-area networks (WBANs), Wireless Sensor Networks (WSNs) and Wireless Personal Area Networks (WPANs).

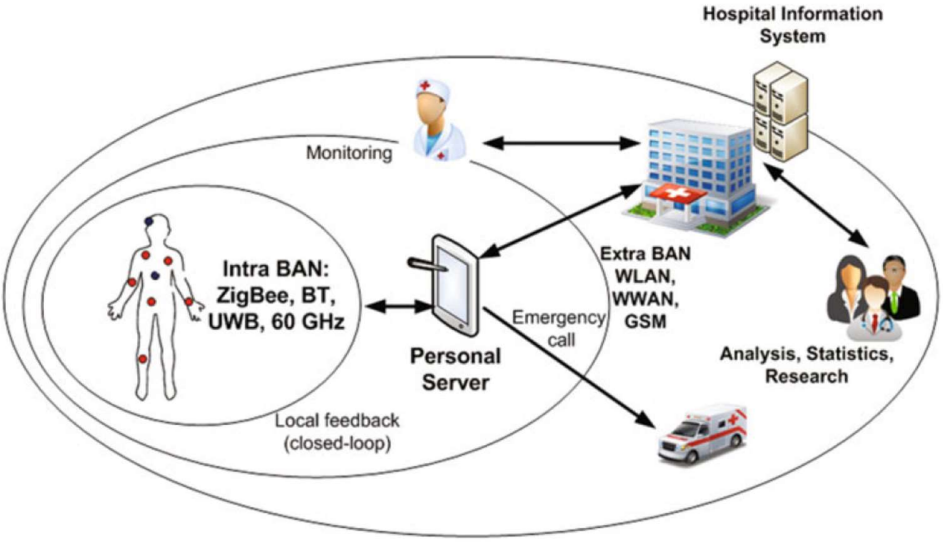

Fig. 1. Patient-centric system.

Body-centric wireless communications technology has numerous applications in healthcare, smart homes, personal entertainment, identification systems, space exploration and the military [5-8]. Battery lifetime in surgically implanted devices still a great challenge as the network has to last for years. Recently, implantable antennas have been largely studied for many sensing and wireless communication applications with tremendous need for integrated wireless powering techniques as energy harvesting/wireless power transfer module to reduce the need for regular battery replacement [9]. Multiband antenna are a potential solution for simultaneous wireless information and power transfer (SWIPT) technique for data rate and the long standby

Peer-reviewed version available at Electronics 2020, 9, 1350; doi:10.3390/electronics9091350

time in the fifth generation (5G) mobile communication systems [10-12]. In order to achieve fully integrated sensors, CMOS technology is employed to design implantable antennas. In such a case, not only the size of antenna itself can be minimized, but also a wireless powering module can be integrated on the same chip.

In this paper, a multiband on-chip antenna is designed and fabricated by UMC 180 nm CMOS technology. The proposed antenna structure is shown in Fig.2, consisting of three layers each in a separate metal layer; an upper meander line (UML), a lower mender line (LML) and a metal ground plane. Compared to normal meander line antenna, the proposed structure doubles tuning frequencies and increases the bandwidth for each tuning frequency. The operation of the proposed antenna resonates at four bands 22 GHz, 34 GHz, 44 GHz and 58 GHz. The broadened bandwidth for each tuning frequency makes it a good candidate for UWB transceivers that need many resonant frequencies for data and power transmission.

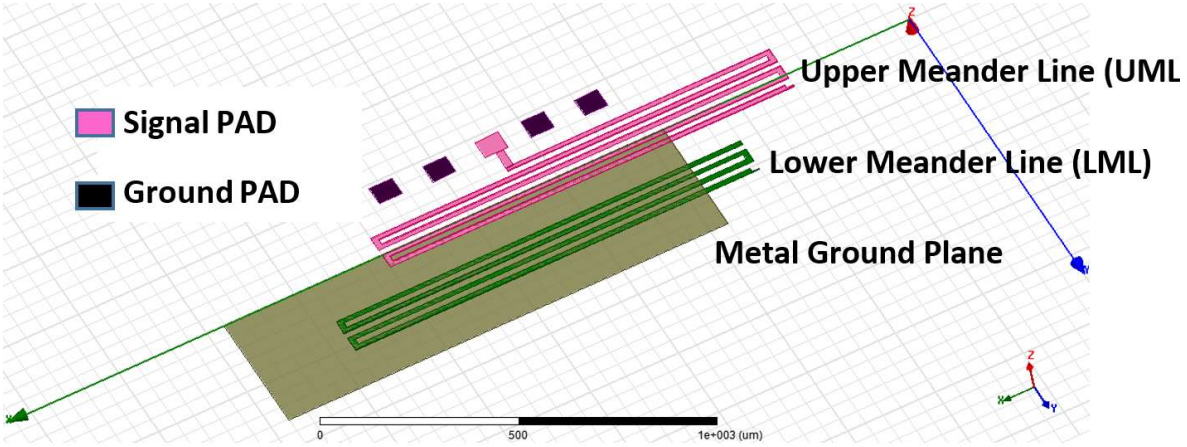

Fig. 2. Proposed dual meander line (DML) antenna structure.

The organization of the paper is set as follows: Section 2 presents a detailed explanation for the DML antenna design. Section 3 present the simulation results for the proposed antenna and compares them with conventional single layer meander line antennas. In section 4, the effect of the human body for both implanted and wearable applications on the antenna performance are demonstrated. The measured results of the proposed

Peer-reviewed version available at Electronics 2020, 9, 1350; doi:10.3390/electronics9091350

antenna and other antenna parameters are shown in section 5. Finally, a conclusion of the paper is shown in section 6.

2. Antenna Configuration and Design

In order to provide good wireless communication from outside the body to inside, factors such as high tissue conductivity, biocompatibility and small antenna size must be taken into consideration. Furthermore, simulation models and physical models are also important to predict the behavior of the antenna in the presence of human-body. The most commonly used models are one-layer models and three-layer models, which were compared in [13] and the results showed that the measured input parameters can be quite different from the real ones if the antenna is to be implanted in the fat layer, otherwise, no significant differences were observed. The dual meander line (DML) antenna is fabricated using UMC180 nm CMOS process. The technology layers consist of a low resistivity Silicon substrate, six metal layers embedded in inter-dielectric layers, with the upper metal layer M_6 being covered with a dielectric passivation layer. As shown in Fig.3, the proposed DML configuration is implemented at two stacked layers, the upper two turns of meander line (UML) at metal layer M_6 and two turns of the lower meander line (LML) at metal layer M_4. The presence of the LML increased the total antenna length which reduced the fundamental resonant frequency when compared to the single meander line (SML) by 20%. A sheet of metal is added as a ground plane to increase bandwidth with an area of 1525 μm×250 μm implemented at the bottom metal layer M_1 and connected to four ground PADs. Both meander line layers have identical structure, line finger has a line width 15 μm, line length 1150 μm line spacing 20 μm between each two fingers in the same layer. The UML has five fingers while the LML has only four fingers. The LML has same alignment as the UML but shifted by 17.5μm, which increases the number of tuning bands. A signal PAD and four ground PADs each 80 μm×60 μm are set and separated by 150 μm. The ground layer is connected to the four ground PADs

Peer-reviewed version available at Electronics 2020, 9, 1350; doi:10.3390/electronics9091350

through four vias. The UML has a 50 Ω line connection with the signal PAD and both meander layers are stacked through Via 1.

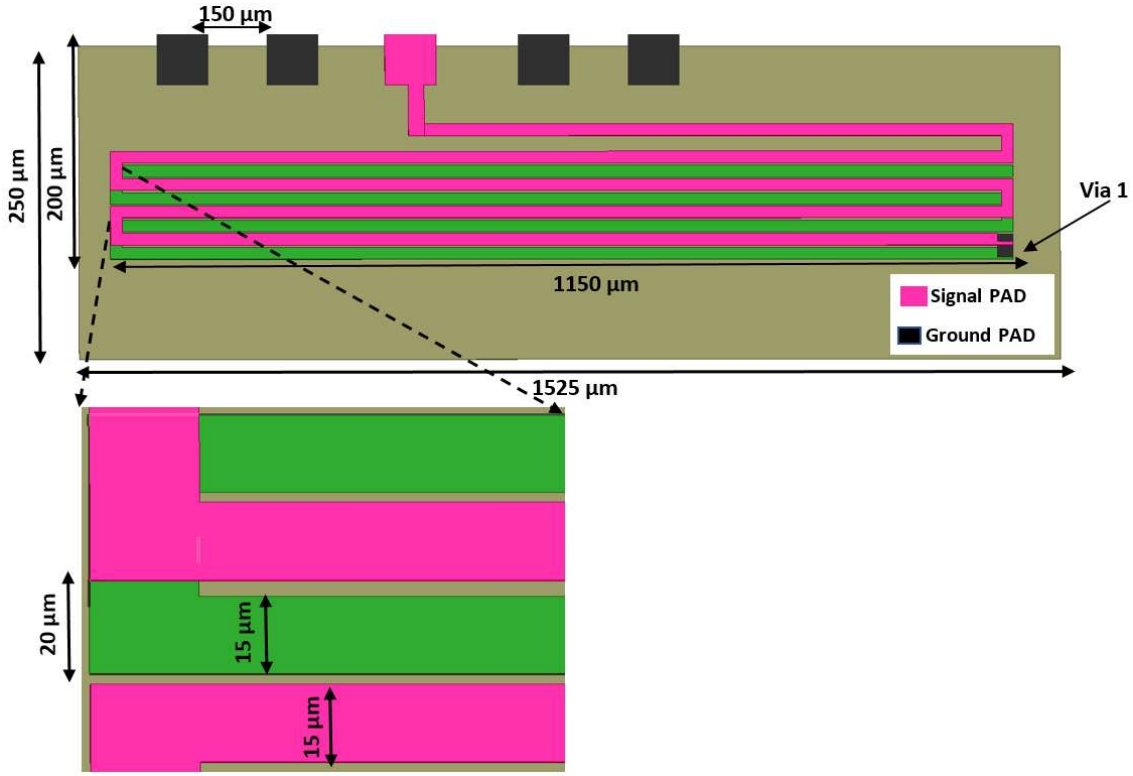

Fig. 3. Configuration of the proposed DML antenna.

3. Antenna Performance Results

The design and performance of the DML antenna are measured using a high frequency structure simulator (HFSS) ver. 15 which is a three-dimensional electromagnetic field simulator. Simulation results show that the proposed structure has four bands of operations. The First band at 22 GHz with bandwidth extended from 20 GHz to 25 GHz, the second band at 34 GHz with bandwidth extend from 30 GHz to 36 GHz, the third band at 44 GHz with bandwidth extend from 42 GHz to 46 GHz and the fourth band at 58 GHz extended from 55 GHz to 63 GHz. To investigate the effect of the proposed dual meander structure, simulation for only a single meander line (SML) antenna located at the metal layer M_6 with same previous dimensions were carried out. The results show that the resonant frequency of SML at 28 GHz is reduced to 23 GHz for DML and the two

Peer-reviewed version available at Electronics 2020, 9, 1350; doi:10.3390/electronics9091350

higher resonant frequencies of SML at 43 GHz and 56 GHz with narrowed bandwidth reduced to 34 GHz and 47.5 GHz with broadened bandwidth for the DML antenna, respectively. Simulated reflection coefficients for both DML and SML antenna are shown in Fig. 4(a), while the resulting input impedance both real and imaginary are shown in Fig. 4(b). Simulations show that the existence of the lower meander line doubles the number of operational bands and improves the bandwidth for each band. The current distribution at different resonant frequencies on the two meander lines surface of the proposed antenna are shown in Fig.5.

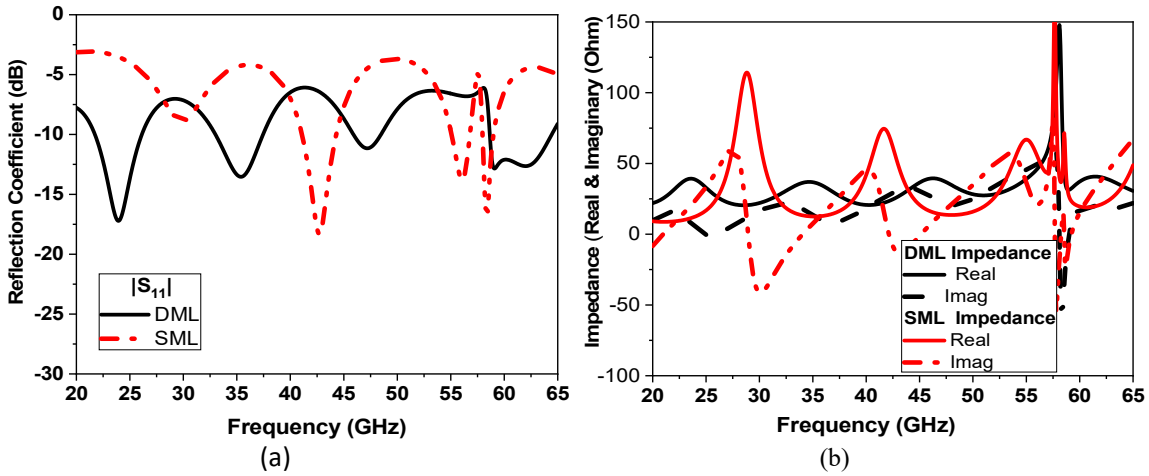

Fig. 4(a) Reflection coefficient versus frequency of the proposed DML and SML antenna (b) Input impedance Real and Imaginary.

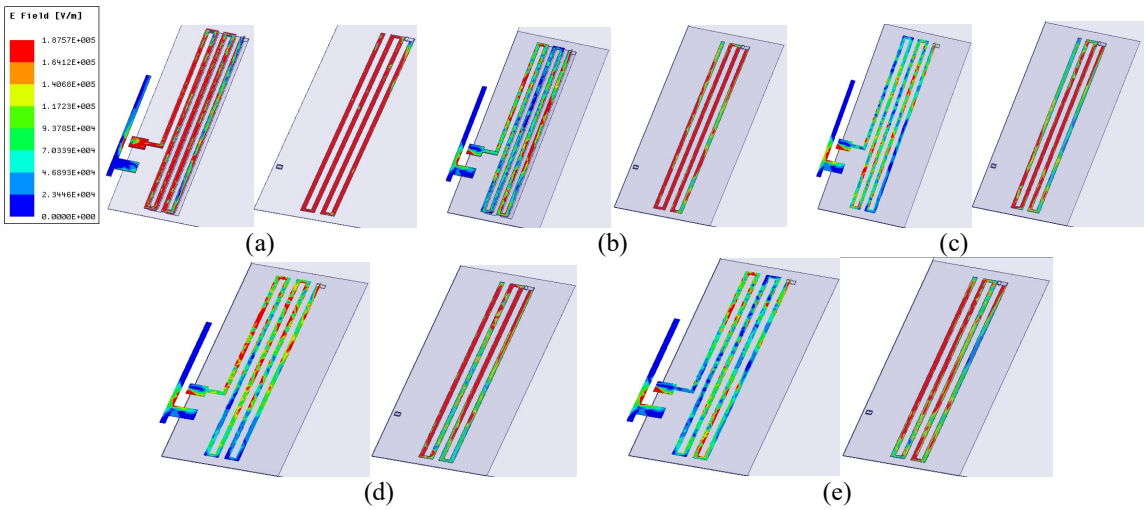

Fig. 5. The surface current distribution of the proposed DML antenna on the two meander lines at different resonant frequencies (a) 22 GHz, (b) 34 GHz, (c) 44 GHz, (d) 58 GHz and 60 GHz.

Peer-reviewed version available at Electronics 2020, 9, 1350; doi:10.3390/electronics9091350

4. Analysis of Human-Body Effect

Body centric networks (BCNs) are mainly used in personal health care in 5G and IoT. The major field in this area is to monitor a large number of patients and control a huge number of sensors with high data rates. The 5G band from 57 to 64 GHz has received much interest for BCN. To check antenna performance for wearable WBAN applications, two scenarios are tested. In the first scenario, the proposed antenna is implanted inside human-body and in the second scenario, the antenna is placed outside human-body with different separation as shown in Fig. 6. The dielectric properties of the human body are characterized up to 65 GHz based on the extrapolation of the data obtained through measurements up to 20 GHz [14], [15]. Single relaxation time of Debye model is considered good accuracy for modelling the permittivity data from 15 GHz to 65 GHz frequency range [16]. The effect of the human body has been added to the proposed DML antenna as a single effective layer with thickness 300 μm, relative dielectric constant ε_r= 11 and effective conductivity δ=2 S/m, by setting frequency dependency with Debye model input in the HFSS simulator. The reflection coefficient magnitude and phase are calculated as shown in Fig.7.

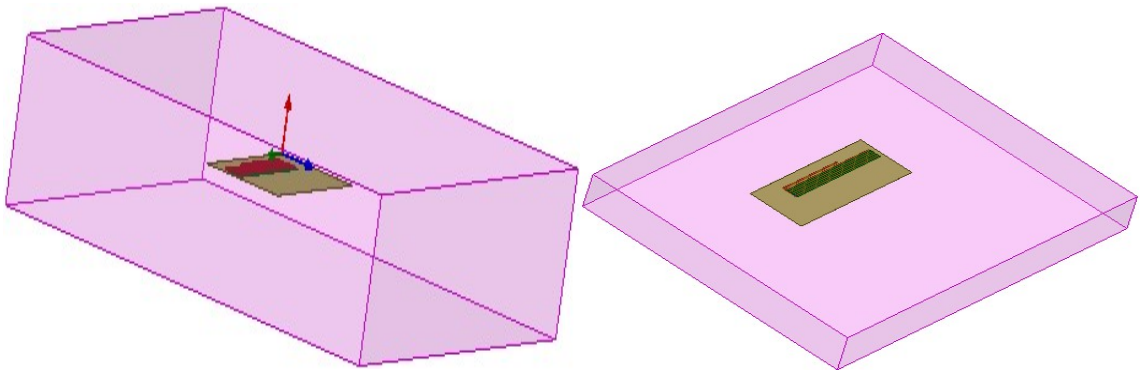

(a) (b)

Fig. 6 Proposed antenna evaluation scenarios (a) Inside human-body and (b) Outside human-body.

The results show that when the human body effect is presented, the antenna impedance matching is more significant for implanted of the antenna inside the human-body. The resonant frequency is shifted down and the operating bandwidth is increased. The other parameter studied is the reflection coefficient phase, which is slightly changed when the antenna is placed outside human-body, and it is abruptly changed when the antenna is implanted in the human-body. The

Peer-reviewed version available at Electronics 2020, 9, 1350; doi:10.3390/electronics9091350

variation of results is due to the conductor layer of the human-body which adds extra load on the antenna surface and changes in the electrical properties of the substrate. However, when the antenna is implanted in the human-body it becomes more dispersive so the operating bandwidth at -7.5 dB (VSWR ≤ 2.5) impedance matching extended from 20 GHz to 45 GHz and from 57 GHz up to 65 GHz. However, in both simulation scenarios, the antenna bandwidth is still operated in the selected bands of operations.

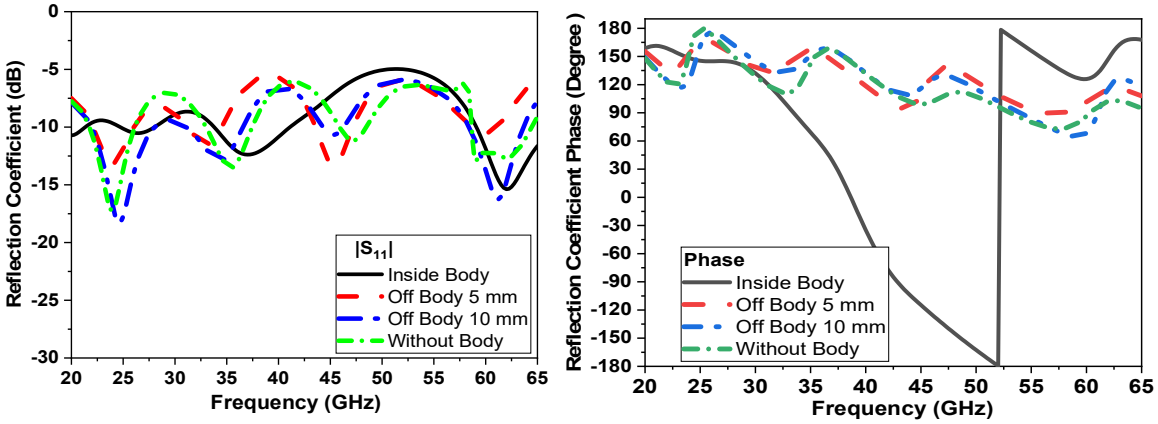

(a) (b)

Fig. 7 (a) Reflection coefficient versus frequency of the DMLantenna with and without humanbody (a) Magnitude and (b) Phase.

5. Measurement of the Proposed Antenna

The proposed DML antenna reflection coefficients are measured in the microstrip Lab, at the Electronics Research Institute. The reflection coefficient achieved by using on-wafer probing and the setup composed of one GSG 67 GHz PicoProbe-RF probe (pitch: 150 µm) and ZVA67 Rohde and schwarz vector network analyzer from 10 MHz to 67 GHz as shown in Fig. 8(a). The fabricated UMC180 nm die (miniasic 1525µm×1525µm) was fixed at PM5 KurlSuss manual probe-station. The photo of the fabricated antenna is shown in Fig. 8(b) with four ground PADs which are connected to the ground metal layer M_1. Fig. 9(a) shows the comparison between the

Peer-reviewed version available at Electronics 2020, 9, 1350; doi:10.3390/electronics9091350

simulated and measured reflection coefficients of the proposed antenna.

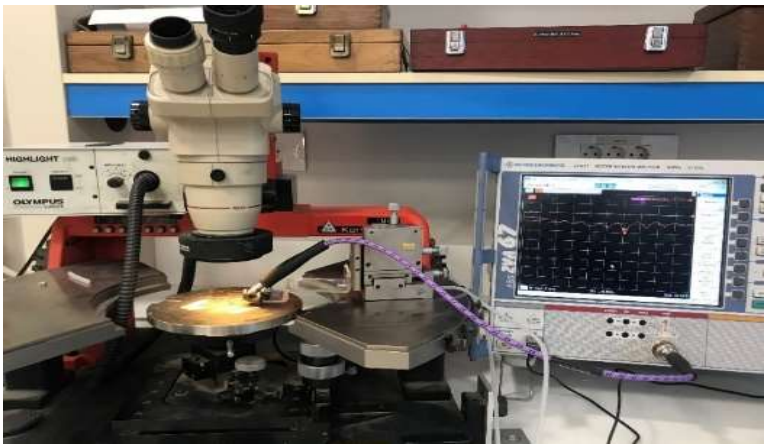

(a)

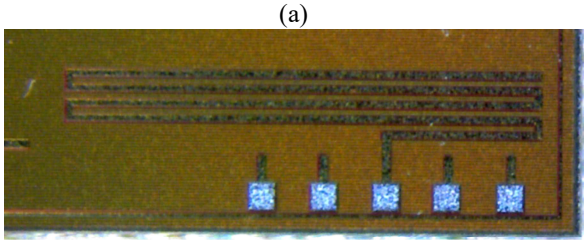

(b)

Fig. 8. (a) The setup of the reflection coefficient measurement and (b) the photo of the fabricated antenna.

There is a good agreement between the start and the end of the designed antenna bandwidth. The simulated 3D polar radiation pattern of the realized antenna gain at four resonant frequencies 22 GHz, 34 GHz, 44 GHz and 58 GHz are shown in Fig. 10(a) to (d), respectively. The normalized 2D radiation pattern of the proposed antenna in the presence of the human body is compared to an absence of the human body at two main coordinates $\varphi = 90^0$ and $\theta = 90^0$ as shown in Table 1 at different resonant frequencies.

Peer-reviewed version available at Electronics 2020, 9, 1350; doi:10.3390/electronics9091350

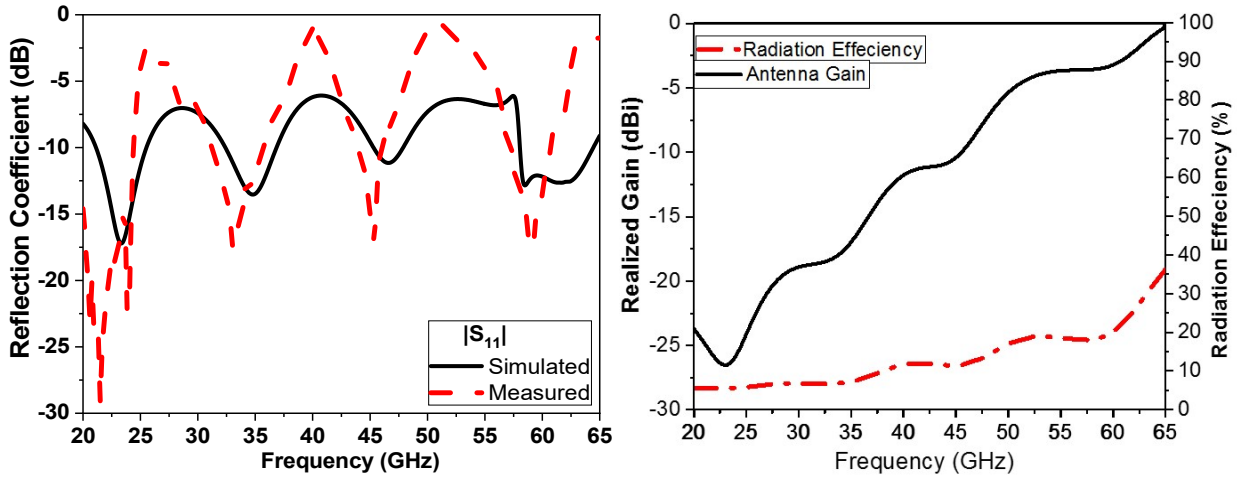

(a) (b)

Fig. 9. Proposed antenna performance versus frequency (a) Measured and simulated |S11| and (b) Gain and radiation efficiency.

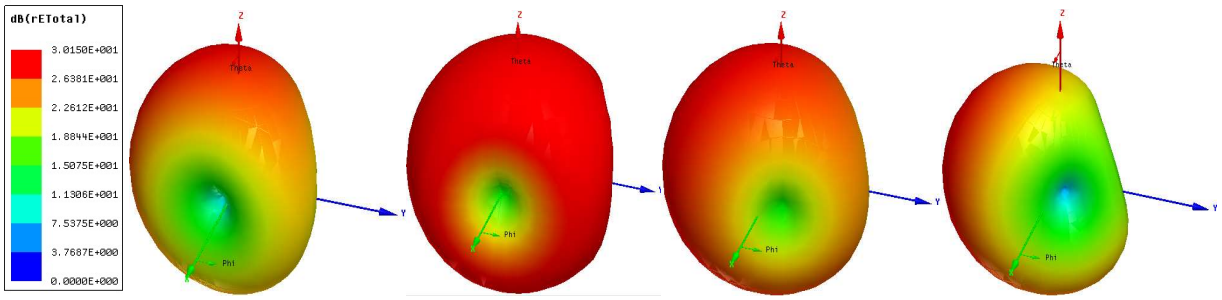

(a) (b) (c) (d)

Fig. 10. 3D Radiation pattern and antenna gain at 22 GHz, 34 GHz, 45 GHz and 58 GHz.

Table 2 shows the performance comparison between the proposed antenna and other previous literature reviews of the integrated antennas operating within the frequency range. In the 60 GHz band, the proposed DML antenna indicates a comparable gain with [18] and [20] with larger bandwidth and achieved multiband of operation. While [22] and [21] are lower gain and single band of operation at frequency higher than the proposed antenna, both antennas have the same efficiency (35%) at 65 GHz range. In references [17] and [18], antennas resonate at 24GHz but with narrow bandwidth and a larger area than the proposed antenna. While [19] and [20] have the largest antenna size area with a high gain. The proposed antenna has low antenna gain at lower frequency; this can be explained due to the small area which reduces the aperture area of the antenna. The

Peer-reviewed version available at Electronics 2020, 9, 1350; doi:10.3390/electronics9091350

proposed antenna is compact when compared to other structures and it has a large number of operational bands. The multiband of operation with wideband bandwidth makes the proposed antenna a good choice for BCN to cover a large number of sensors for many patients. Essentially, the antenna provides a wireless power transfer system that can be integrated for battery less applications.

Table 1: The 2D polar radiation pattern — without human-body, - - - with human-body at different resonant frequencies.

Plane	22 GHz	34 GHz	45 GHz	58 GHz
φ=0°	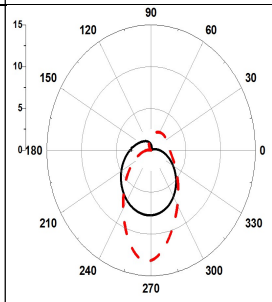	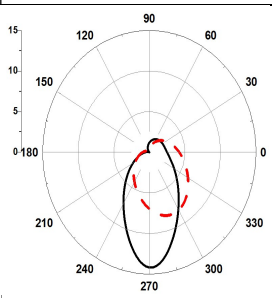	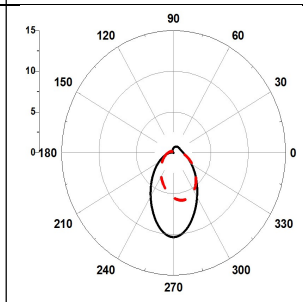	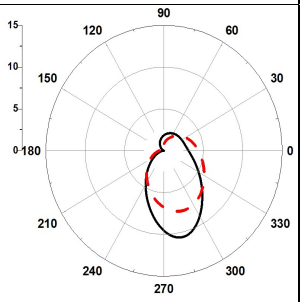
θ=90°	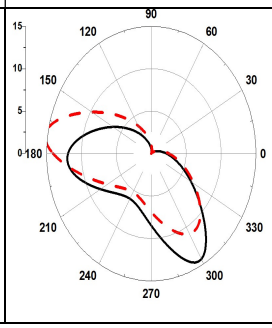	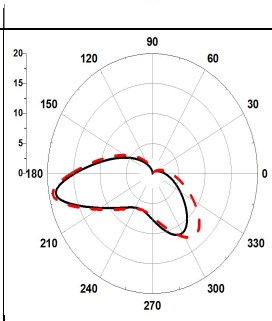	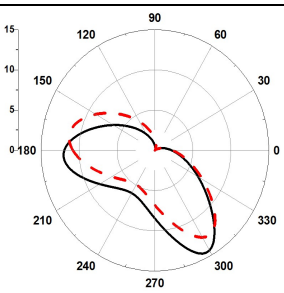	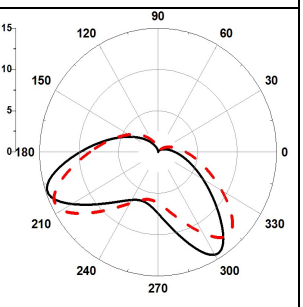

Table 2: Comparison of the proposed antenna with other on-chip antennas

Ref	[17]	[18]	[19]	[20]	[21]	[22]	This work
Freq. GHz	24	24/60	40-50	60	94	67	22/34/44/58
Gain dBi	-8	-9/-1	0.8 to 3.3	-3.2	-2.71	-8	-20/-15/-10/-1
BW GHz	--	0.18/0.7	5.3	5.5	15	4	5/6/4/8

Peer-reviewed version available at Electronics 2020, 9, 1350; doi:10.3390/electronics9091350

Area mm²	3 mm length	0.794	1.87	2.25	0.22	0.875	0.23 mm²
Tech.	0.13µm CMOS	0.13µm CMOS	0.18 µm CMOS	0.18 µm CMOS	IHP 0.13µm Bi-CMOS	0.18µm CMOS	0.18 µm CMOS

6. Conclusion

In this paper, a compact of dual meander line integrated antenna for multiband biomedical applications is proposed. The proposed antenna consists of two stacked layers of meander lines and a ground metal layer. The DML structure increased the number of tuning bands with broadening bandwidth which make it suitable for high data rate 5G body centric network (BCN) applications. The proposed antenna has suitable gain and efficiency in the operational bands 44 and 60 GHz band when compared to different on chip antennas. The proposed antenna has small area by 20% from traditional meander line antennas for easily integration with implantable/wearable systems. The proposed antenna has acceptable performance when it is implanted or worn on the human body.

References

[1] M. Ali, M. Sawan, H. Shawkey, A. Zekry "FM-UWB transmitter for wireless body area networks: Implementation and simulation," IEEE International Symposium on Circuits and Systems (ISCAS, 2016.

[2] P. Hall, "Advances in antennas and propagation for body centric wireless communications", Antennas Propag.(Eu CAP 2010), Barcelona, Spain, April 12–16, 2010

[3] Q. H. Abbasi, M. Ur-Rehman, K. Qaraqe, and A. Alomainy, "Advances in body-centric wireless communication: Applications and state of the art," the IET, (UK), 2016.

[4] Mehmet R.Yuce, "Ultra-wideband and 60 GHz communications for biomedical applications", springer science business media, New York, 2014.

[5] Y. Hao, "Antennas and propagation for body centric wireless communications," IEEE International Conference on Microwave Technology & Computational Electromagnetics, May 2011.

[6] Z. Liu, Y. Guo "Dual band low profile antenna for body centric communications," IEEE Transactions on Antennas and Propagation, vol. 61, Issue: 4, April 2013.

Peer-reviewed version available at Electronics 2020, 9, 1350; doi:10.3390/electronics9091350

[7] H. Sabti, D. Thiel, "Node Position Effect on Link Reliability for Body Centric Wireless Network Running Applications," IEEE Sensors Journal, vol. 14, no. 8, August 2014.

[8] M. U. Rehman, N. A. Malik, Xiaodong, Q. H. Abbasi, Z. Zhang and N. Zhao, "A low profile antenna for millimeter-wave body-centric applications" IEEE Transactions on Antennas and Propagation, vol. 65 , no. 12 , pp. 6329 – 6337, Dec. 2017.

[9] S. Ladan, A. Guntupalli and K. Wu, "A high-efficiency 24 GHz rectenna development towards millimeter-wave energy harvesting and wireless power transmission," IEEE Transactions on Circuits and Systems I: Regular Papers, vol. 61, Issue 12, 2014.

[10] J. Huang, C. Xing, C. Wang, "Simultaneous wireless information and power transfer: technologies, applications, and research challenges," IEEE Communications Magazine, vol.55, Issue: 11, Nov. 2017.

[11] X. Wang, M. Cenk Gursoy, I. Guvenc, "Simultaneous wireless information and power transfer in UAV-assisted cellular IoT networks," IEEE 17th Annual Consumer Communications & Networking Conference (CCNC) 2020.

[12] X. Xu, A. Özçelikkale, T. McKelvey and M. Viberg, "Simultaneous information and power transfer under a non-linear RF energy harvesting model," IEEE International Conference on Communications Workshops (ICC Workshops) 2017.

[13] E. Porter, H. Bahrami, A. Santorelli, B. Gosselin, L. A. Rusch and M. Popović, "A Wearable microwave antenna array for time-domain breast tumor screening," in *IEEE Transactions on Medical Imaging*, vol. 35, no. 6, pp. 1501-1509, June 2016.

[14] S. Gabriel, R. W. Lau, and C. Gabriel, "The dielectric properties of biological tissues: II. measurements in the frequency range 10 Hz to 20 GHz," Physics in Medicine and Biology, vol. 41, no. 11, pp. 2251–2269, 1996.

[15] "Dielectric properties," ITIS website, http://http://www.itis.ethz.ch/virtualpopulation/ tissue-properties/database/dielectric-properties).

[16] D. N. Elsheakh and M. F. Iskander, "Circularly polarized tri-band printed quasi-Yagi antenna for millimeter-wave applications", International Journal of Antennas and Propagation, pp. 1-10, vol.15, 2015.

Peer-reviewed version available at Electronics 2020, 9, 1350; doi:10.3390/electronics9091350

[17] C. Cao, Y. Ding, X. Yang, J. Lin, A. Verma, J. Lin, F. Martin and Kenneth K. O, "A 24-GHz Transmitter with an On-chip Antenna in 130-nm CMOS," IEEE Transactions on Antenna and Propagation, vol. 56, no. 2, Feb. 2008.

[18] J. Huang, J. Wu, Y. Chiou and C. Jou, "A 24/60GHz Dual-band millimeter-wave on-chip monopole antenna fabricated with a 0.13-μm CMOS Technology," IEEE International Workshop on Antenna Technology, May 2009.

[19] Y. Song, Q. Xu, Y. Tian, J. Yang, Y. Wu, X. Tang, et al., "An on chip frequency-reconfigurable antenna for Q-band broadband applications," IEEE Antennas Wireless Propag. Lett., vol. 16, pp. 2232-2235, 2017.

[20] L. Wang and W. Z. Sun, "A 60-GHZ differential-fed circularly polarized on-chip antenna based on 0.18-m COMS technology with AMC structure," IET International Radar Conference, pp. 1-4, Hangzhou, 2015.

[21] M. S. Khan, F. A. Tahir and H. M. Cheema, "Design of bowtie-slot on chip antenna backed with E-shaped FSS at 94 GHz," 2016 10th European Conference on Antennas and Propagation (EU CAP), pp. 1-3, Davos, 2016.

[22] Y. Song, Y. Wu, J. Yang and K. Kang, "The design of a high gain on-chip antenna for SoC application," Advanced Materials and Processes for RF and THz Applications (IMWS-AMP), 2015 IEEE MTT-S International Microwave Workshop Series on, pp. 1-3, Suzhou, 2015.